Chapter 4. The Two-Dimensional Inverse Problem

Introduction

Up to this point we have dealt primarily with the theory and practice of computing synthetic reflection seismograms from a known reflector model. We have included the wave effects of focusing and diffraction in the synthesis of primary and multiple reflected arrivals. This, the forward problem, represents a useful new tool in the analysis of diffracted multiple phenomena through various model studies. In an interpretive sense, one can conceive of procedures for interactively or iteratively adjusting the model to obtain close agreement between the synthetic and field data. Such schemes of organized trial-and-error are to be found applied to many geophysical problems.

This type of "inversion" approach usually involves developing a functional relationship between the observable results and the model parameters. Linearizing the system of equations, an initial model is then iterated in order to improve some quadratic measure of the errors between the observed and calculated data. For an arbitrarily complex medium, the system of equations needed for modelling 2D reflection seismograms becomes immense. To make the problem tractable numerically, the common approach is to extract a modest amount of information, such as reflection picks, for use as "data" in the inversion algorithm. We will not be considering such techniques here.

It is the central point of this thesis that diffracted and focused primary and multiple reflected energy represents valuable signal information essential to high resolution mapping of reflectors. Furthermore,

this information can be used directly, within the framework of the theory developed, to properly map subsurface reflectors.

Before proceeding with the discussion of the inverse problem we shall recall and discuss the more important assumptions and approximations made up to this point. This will serve to delineate the scope (and applicability) of the problem we will be considering. The two-dimensional assumption was initially made on the premise that reflection seismic profiles are shot perpendicular to the presumed geologic strike. In addition, the point should be made that in the absence of integrated cross-shooting or 3D coverage this is perhaps the best assumption which can be made. In any case, out-of-plane reflections and energy losses are not modelled by our equations.

Our use of velocity is only concerned with migrating diffracted primary and multiple waves. Choosing the "depth" sampling function to be $\Delta z = \tilde{v}\, \Delta t / 2$ was an artificial way of preserving the one-to-one correspondence between points on the model C and points on the seismograms R. Actually this results in C being termed a migrated time-section (or reflection coefficient time-map) as opposed to a depth-section. We may consider a migration process of consisting of two separate operations. One is concerned with the movement of diffracted and focused energy while the other deals with the broader aspect of velocity related travel time anomalies. In the former, we use the migrating partial differential equation to collapse diffraction hyperbolas to points and diffuse focused regions. In the latter, we do a final stretching of the time coordinate in accordance with a velocity profile to yield a depth section.

This distinction is clarified in referring to Figure 4-1. Frame (a) represents a depth section of a low velocity mass bounded by reflectors 1 and 2. Frame (b) is the reflection time-section on which the velocity pull-down due to the excess low velocity path in the anticlinal crest can be noted. Note also the diffraction hyperbolas arising from the fault boundary. The migrating differential equation applied to the data of (b) yields a migrated time-section (c). Application of a velocity $\tilde{v}(x,z)$ in stretching the time axis gives a migrated depth-section. In the forward problem we begin with a reflection coefficient time-section C and compute the reflection seismograms R. The inverse problem, in this context, consists of deducing C from the observed reflected primary and multiple waves R.

As in the one-dimensional algorithm, we will have need for an estimate of the source waveform inverse. In the forward problem we specified both the magnitude and waveform of the initial surface disturbance. Here we assume that this information is likewise available, either indirectly through an estimate (based on the relationship between primary and multiple waves) or, perhaps, directly measured. The source waveform inverse, when applied to the data, calibrates the seismograms to those of a unit magnitude, impulsive source.

A basic assumption in developing the equations for upward and downward propagation was that we restrict consideration to those waves travelling at angles close to the vertical. This led to a simplification of the continuation equations and resulted in a numerically manageable algorithm. We might expect that including the higher-accuracy term ∂^t_{xxz} would enable us to include the wide-angle paths. This would be true in homogeneous regions. However, we should note

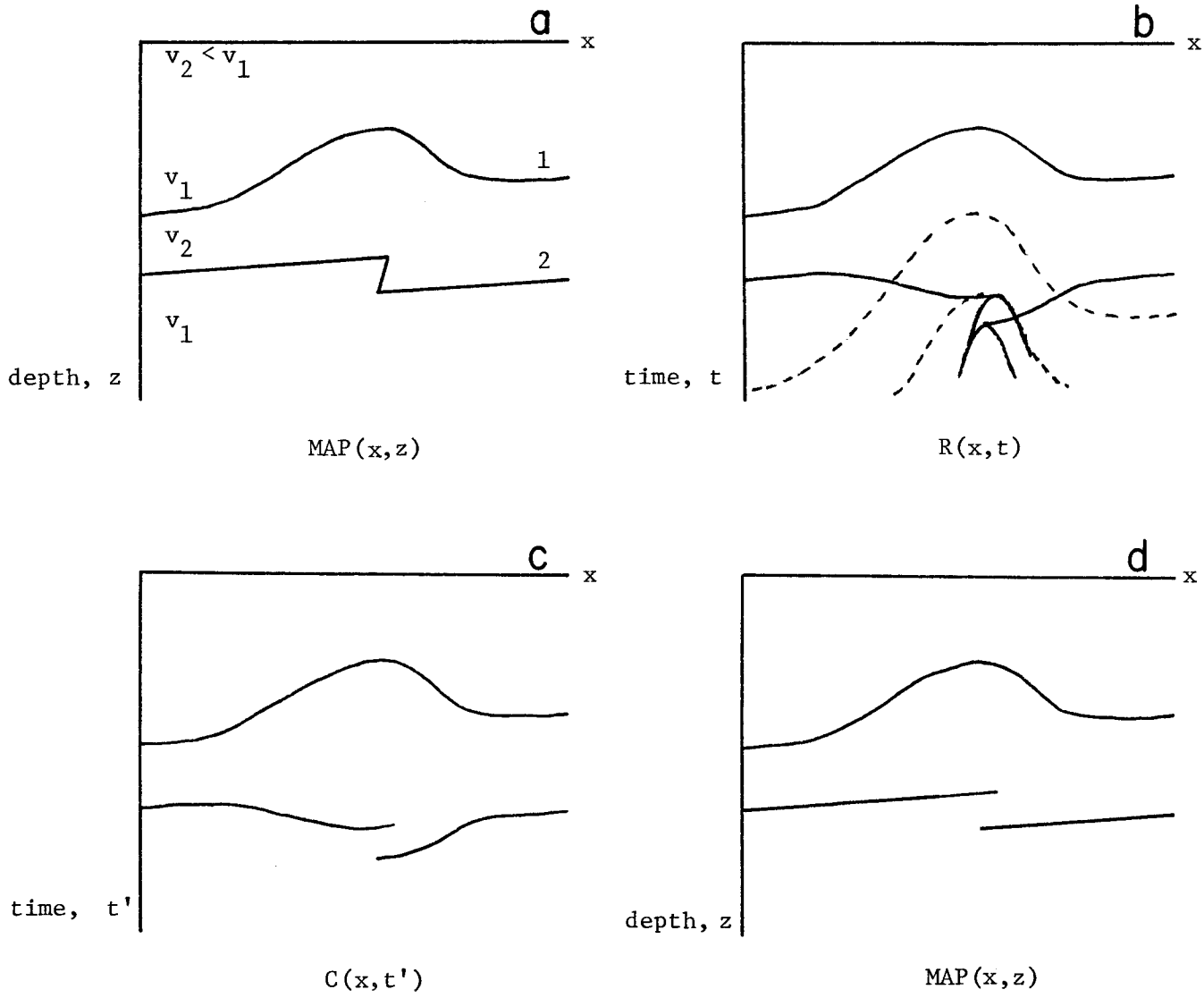

Figure 4-1 Illustrating the steps involved in inverting reflection seismic data. Frame (a) represents a depth section of a low velocity zone bounded by reflecting interfaces 1 and 2. Frame (b) is reflection time-section as observed at zero offset. Note the characteristic velocity pull down due to the excess low velocity medium. Also note the diffraction hyperbolas generated by the sharp fault boundary. Multiples are indicated by dashed lines. The migrating partial differential equation applied to the data of (b) yields a migrated time section (c). Multiple reflections are modelled by our equations and are properly extinguished in going from (b) to (c). Application of the velocity $\tilde{v}(x,z)$ in stretching the time axis gives a migrated depth-section (d). Our inversion technique consists of deducing a reflection coefficient time-section C from the reflection seismograms R.

that in perturbing the solution about vertical paths, the coupling of the waves is expressed in terms of vertical derivatives of the velocity. That is, the reflectors are defined in terms of normal incidence reflection coefficients; the reflection magnitude is independent of incident angle. The truth is that the reflection coefficient is a function of angle. Fortunately, the variation in magnitude is slow near normal incidence (Muskat and Meres, 1940).

The uncertainty in the reflection coefficient, and, additionally, the existence of converted waves may be reduced by dealing with only the narrow-beam ($< 15° \sim 20°$) paths. For the usual reflection geometry involving moderate subsurface dips this condition is reasonable for recordings due to a plane wave source. Thus, the inversion technique will be based on the narrow-beam equations of (3-31) with an initial plane wave source $E(x) = 1$.

Dealing with Causality

The reflection seismograms observed at the surface of the earth provide necessary boundary conditions for downward continuing both the up and downgoing waves. In the case of downgoing waves this is also sufficient information (together with the migration velocity) for projecting the waves to arbitrary depth. Thus, equation (3-31b) may be used, with the major recursion over time or depth, to compute the D wave field everywhere in the (z,t'') plane. Considering the downgoing waves to be known everywhere of interest, we now must focus on the important upcoming wave equation.

Physically, when time flows forward, the differential equation (3-31a) propagates upcoming waves toward the surface (decreasing z). To propagate upcoming waves back down into the earth (increasing z), time must run backwards. Thus, in the upcoming wave equation time and depth may naturally move in either direction, but not the same

direction. Conversely, for the downgoing wave equation time and depth must flow in the same direction. In the physical world, where time runs forward, this is a statement of causality. In the computer, where time can go either way, it becomes a requirement for stability. The forward problem, either done in the computer or in the field, requires time to run forward and the up and downgoing waves travel in opposite directions. In the inverse, we will use the computer to project both waves downward, resulting in time running in opposite directions with respect to the separated wave fields.

The upcoming equation (3-31a) is approximated by the finite difference operator (3-43).

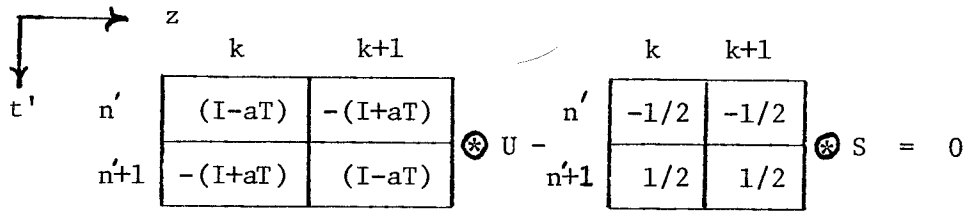

Recall that the source term S was defined as the cross product of the reflection coefficients and the downgoing wave $S_k^{n'} \triangleq C_k D_k^{n'-k}$. For the moment assume that S is known. The stable direction of convolution for the inverse is in solving for $U_{k+1}^{n'}$. The major (outer) recursion proceeds from the surface down to the deepest detectable reflector, i.e., $k=0$, $k=1$, $k=2$, $\cdots$. The minor (inner) recursion integrates the waves, at a constant depth (k), from $t'=\infty$ to the first arrival of the downgoing wave. In practice we only record for a few seconds, say t'_{max}. However, usually this is sufficient time for the reflected waves to fall well below a detectable level. Thus, assuming that the upcoming waves vanish for $n'> n'_{max}$ we integrate $U_k^{n'}$ back in time: $n'= n'_{max}$, $n'= n'_{max} -1, \cdots$, $n'= k-1$, $n'= k$ along cells at constant k. Figure 4-2 illustrates the

recursion for the inverse problem as compared to that of the forward. The important thing to note is that we have the observed seismograms $R(x,t)$ as a boundary condition at $z=0$. The entire reflected wave field participates in the calculation. As we integrate up from n'_{max} the upcoming waves are projected down one Δz step.

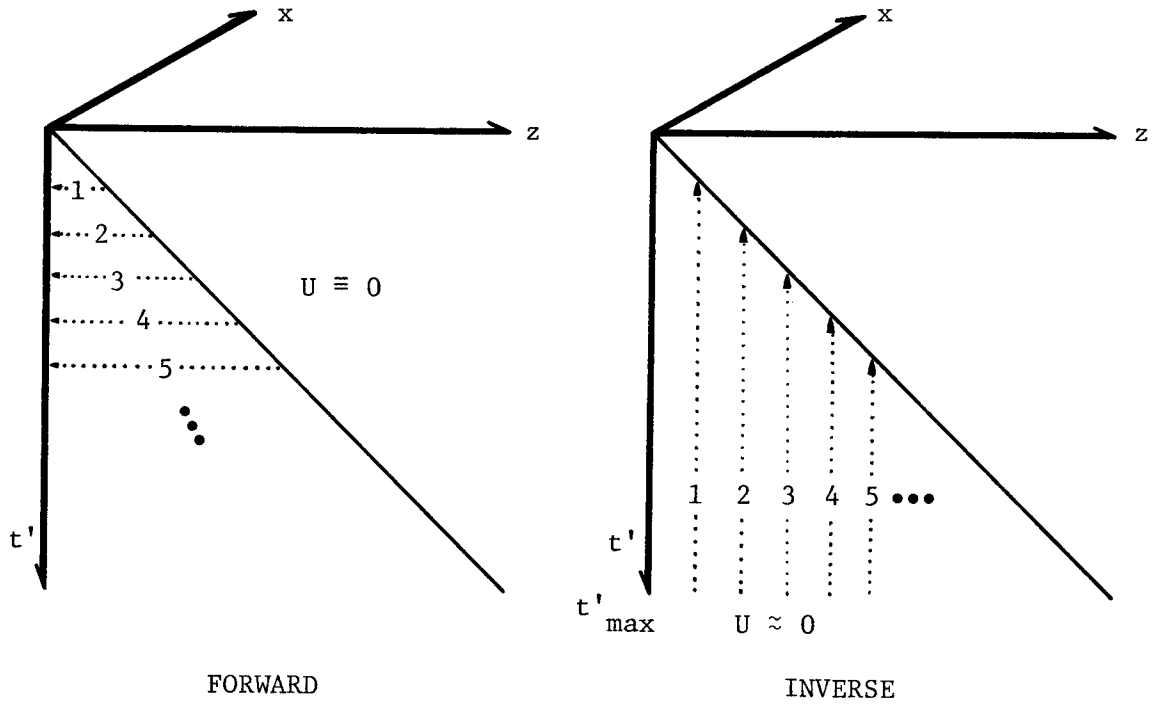

Figure 4-2. Two causal directions exist for propagating upcoming waves as illustrated above. The finite difference operator is used recursively on the U and S (z,t') planes. In the forward problem (left), the major recursion 1, 2, 3, 4, 5 ··· is over time. The minor recursion (arrows) integrates U from the reflectors to the surface. In the inverse problem (right), the major recursion is over depth. The minor recursion integrates the upcoming waves backwards in time, to the first arrival of the downgoing wave, for a particular depth. A boundary condition in the inverse is that upcoming waves vanish after the maximum recording time, t'_{max} . As we integrate up from t'_{max} the upcoming waves are projected down one Δz step.

Knowing how to correctly downward continue upcoming waves through a known medium (i.e., given $C(x,z)$ and computing $D(x,t'')$, the reflected source waves $S(x,t')$ may be determined) is an important part of the inverse problem. The other part arises in the interesting case where C is unknown. In some situations we may have a priori knowledge of the source wave field. This is true for data collected in very deep water where the length of recording encompasses mainly primary reflected energy. For practical purposes it may be assumed here that the downgoing wave consists of just an impulsive plane wave. Thus, S is zero everywhere in the (z,t') plane except along the first arrival trajectory. With $S_k^{n'} = D^o C_k \delta(n'-k)$, U may be integrated up from n'_{max} to $n' = k-1$ neglecting the source term. At the reflector $(n'=k)$ we have, now including the non-zero source term D^oC_k,

$$(I+aT)\, U_k^k - D^o C_k / 2 = (I-aT)(U_k^{k+1} + U_{k-1}^k) - (I+aT)\, U_{k-1}^{k+1}$$

and using $U_k^k = D^oC_k$ we may compute C_k from

$$(I+2aT)\, C_k = 2/D^o \,[(I-aT)(U_k^{k+1} + U_{k-1}^k) - (I+aT)\, U_{k-1}^{k+1}\,] \qquad (4\text{-}1)$$

This represents a special case for the migration or mapping of reflectors in the absence of multiple reflections. In the presence of multiple reflections the downgoing wave is contaminated with reflected energy from the free surface. Subsequent interaction with the reflection coefficients generates source terms after the passage of the first arrival. Thus, in general, we must assume that $S_k^{n'}$ may be non-zero for all n' in the region $k \le n' \le n'_{max}$ of the (z,t') plane.

Principles of Reflector Mapping

The separate continuation of up and downgoing wave fields provides the necessary framework in which a general reflector mapping procedure may be developed. The ability to compute both wave fields at depth is a great advantage in imaging complex reflectors. We may immediately call upon two very basic principles of reflector mapping, applicable over a wide range of situations including the presence of diffracted multiple reflections. The first is the fundamental principle of reflector mapping (Claerbout, 1971b) which states: reflectors exist at points in the ground where the first arrival of the downgoing wave is time-coincident with an upcoming wave. This very useful principle provides an operational definition of a reflecting interface in terms of up and downgoing waves. The second principle which is also of basic importance to the inverse problem is: at any given point in the earth, upcoming waves must vanish for all time prior to the first arrival of the downgoing wave. Both principles are valid for an arbitrary number of reflectors.

These ideas are illustrated in figure 4-3 where we have a surface source E and a reflector at depth z_3 corresponding to receiver location G_3. There are also receivers located above and below the reflector with the observed up and downgoing arrivals displayed with time referenced to the shot. At the reflector G_3 the upcoming wave is time-coincident with the first arrival. Prior to the first arrival of the downgoing wave (left triangular region) the upcoming waves are not observed. The relationship between the waves observed in this coordinate system and the transformed

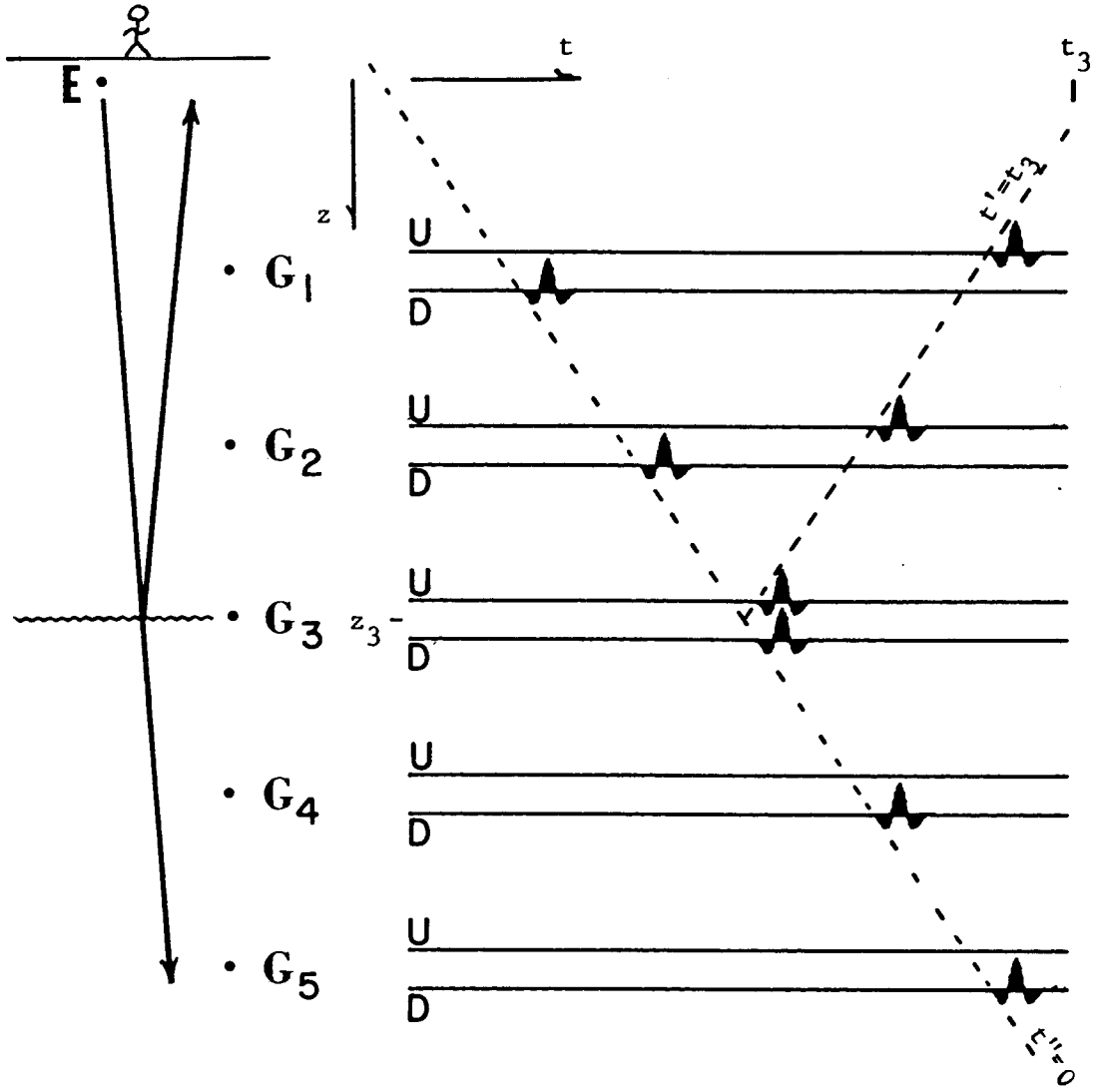

Figure 4-3. Up and downgoing waves observed with buried receivers. A disturbance exits the surface at $t=0$ and is observed passing the receivers $G_1 \ldots G_5$ at progressively later times. At the depth z_3 of a reflector, G_3 receiver records, in time-coincidence, both the upcoming and downgoing waves. Shallower receivers also record both waves. Deeper receivers record only D . The diagonals are lines of constant surface arrival time (t' = const.) for U and lines of constant surface departure time (t'' = const.) for D . The fundamental principle of reflector mapping states that reflectors exist where U and $D(t''=0)$ are time coincident. A second principle is that the upcoming waves must vanish for all time prior to the first arrival of the downgoing wave.

coordinate is,

$$t' = t + z/\bar{v}$$

$$t'' = t - z/\bar{v} \quad .$$

Thus, the two diagonals in the figure represent lines of constant t' (constant surface U arrival time) and $t'' = 0$ (first D arrival time). In the region to the left of the first arrivals, $t < z/\tilde{v}$, the upcoming waves must vanish. This corresponds to the upper triangular region in the (z, t') plane $t' < 2z/\tilde{v}$

Although we may record primary and multiple reflections arriving simultaneously at the surface, all the upcoming waves must vanish below the deepest reflection point consistent with that surface arrival time. Actually, we have used both principles previously in the forward problem. There we used the boundary condition that $U(z,t')$ and $S(z,t')$ were zero to the right (below reflectors) of the first arrival trajectory, $t'' = 0$, in integrating up to the surface. In the inverse we integrate down to the reflector, whereupon further integration past the reflector should cause the upcoming waves to perfectly extinguish. Thus, the second principle provides a performance constraint for the downward continuation of U , while the fundamental principle provides a basis for imaging reflectors from U and D waves. We may think of this as a sort of bootstrap procedure: to downward continue U to a given depth we need the reflection coefficients C for that and all shallower depths; to estimate C at a given depth we need both U and D at that depth.

As the waves are projected back down into the earth they begin to focus on the reflectors. Crossing the reflector the primary waves should exactly image the interface. Simultaneously all multiple waves ending with that same primary path must vanish. Thus, downward continuation of U (including the multiple source term) is both a means of imaging complex reflectors and inverting diffracted multiple reflections. The ability to correctly estimate the reflection coefficients from the waves at the reflectors is essential to the inversion of the multiples.

Estimating Reflectors from the Waves

It suffices to consider the problem of computing U_k and C_k knowing the upcoming wave and reflection coefficient cells one Δz step above: U_{k-1} and C_{k-1}. Convolving backwards in time from t'_{max} the columns of cells $S_k^{n'} = C_k D_k^{n'-k}$ and U_k are unknown.

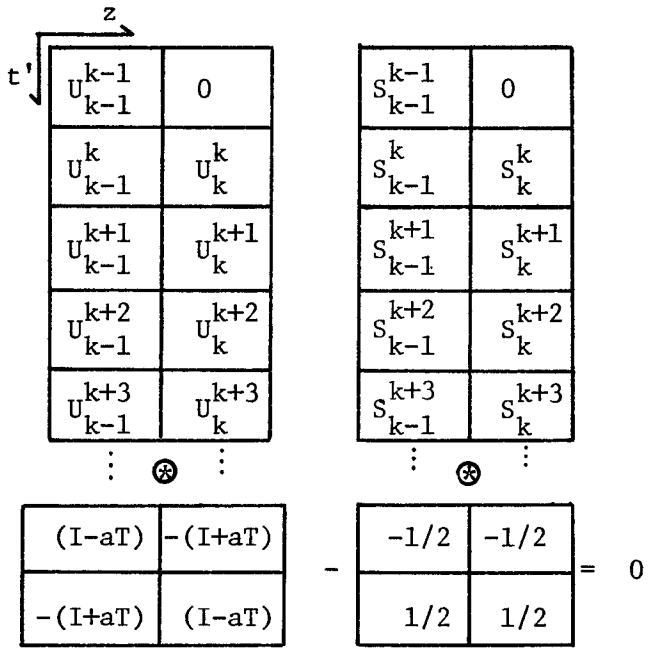

(4-2)

Consider inserting <u>two</u> trial values for the reflection coefficients; say $C_k = +1$ and $C_k = -1$ for all points along the x-axis. With the trial sources of $S_k^{n'} = \pm D_k^{n'-k}$ we integrate the upcoming wave equation up to the first arrival $n'=k$. In the process we excite erroneous upcoming waves, say e^+ and e^- corresponding to the C's of +1 and -1, respectively. Furthermore, continuing to integrate <u>past</u> the time of first arrival we will, if the trial reflection coefficients are incorrect, experience upcoming waves $(e_{-1}^+ , e_{-2}^+ , e_{-3}^+ , \ldots)$ and $(e_{-1}^- , e_{-2}^- , e_{-3}^- , \ldots)$ before the first arrival of the down-going wave. From the erroneous waves we will deduce the true reflection coefficient.

Next, consider forming a linear combination of these two separate experiments

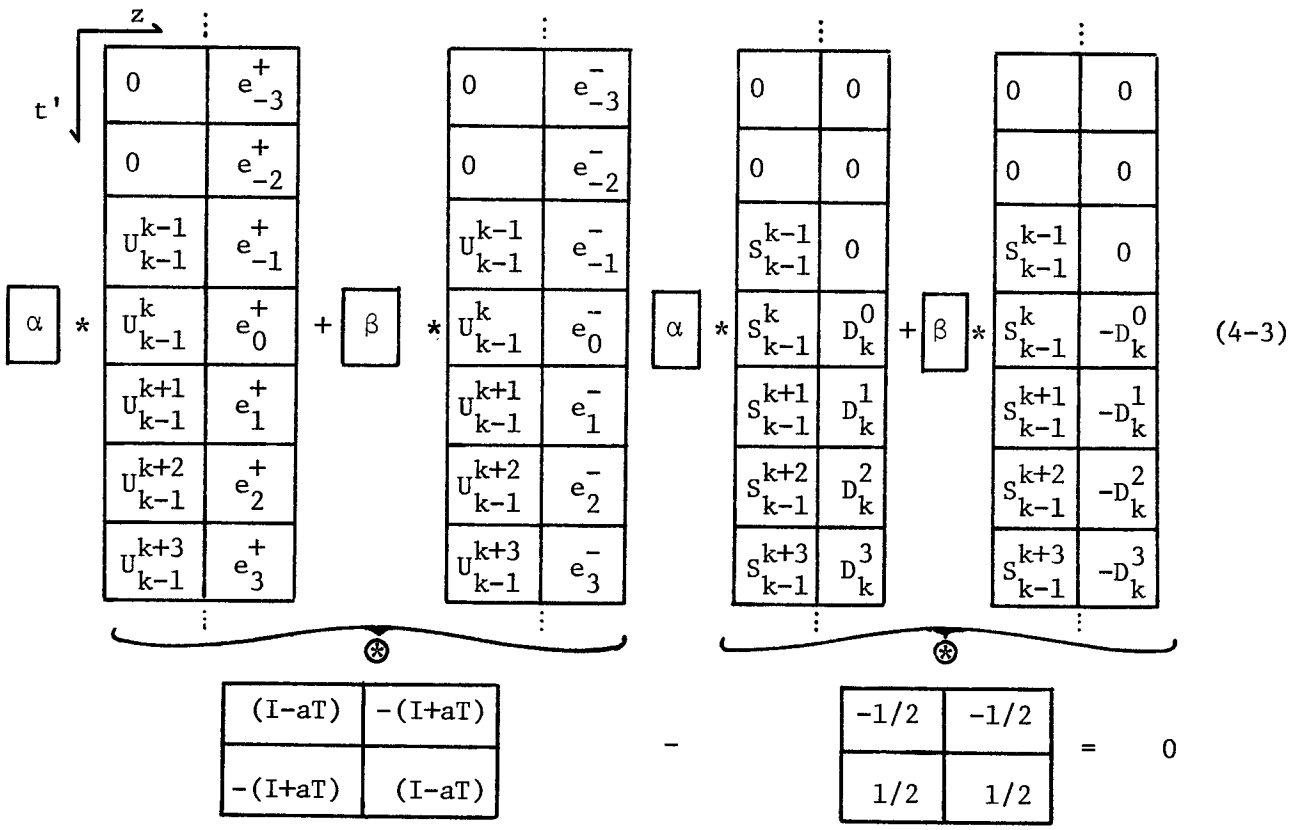

(4-3)

Choose to constrain the combination such that the left-hand, or known, upcoming and source wave columns are unmodified;

$$\alpha + \beta = 1 \tag{4-4}$$

Further, choose the weights such that the right hand source column is the product of the reflection coefficients C_k and the downgoing wave;

$$\alpha - \beta = C_k \, . \tag{4-5}$$

Thus, solving for (α,β) , the proper linear combination expressed in terms of the unknown reflection coefficients is

$$\alpha = (1 + C_k) / 2 \tag{4-6 a,b}$$

$$\beta = (1 - C_k) / 2$$

The equations for the unknown upcoming waves in terms of the erroneous upcoming waves are

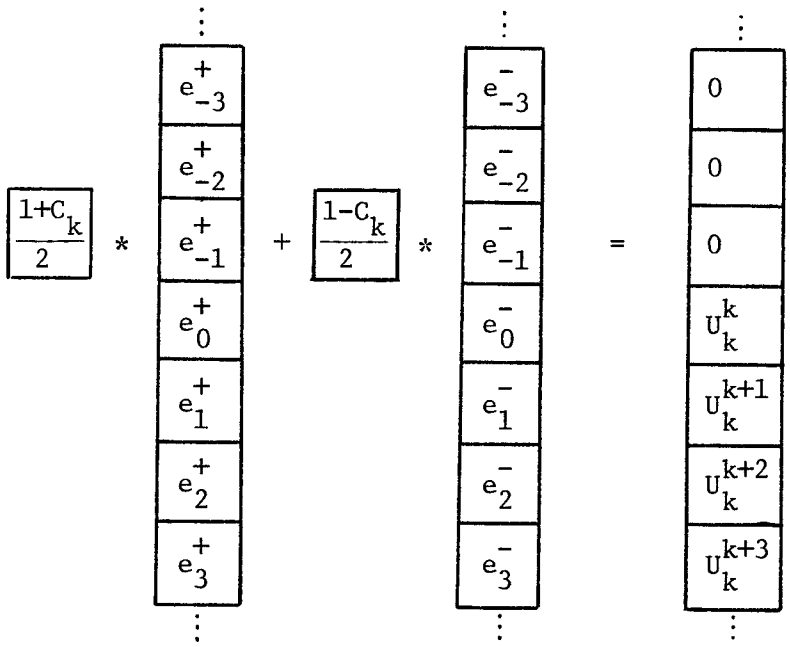

(4-7)

where we have made use of the second principle in specifying the upcoming waves to be zero for $n < k$. From the top set of equations in (4-7) we may derive an estimate of the reflection coefficient. If we were to use just the single equation before the first D arrival, the estimate would be

$$C_k = (e^-_{-1} + e^+_{-1}) / (e^-_{-1} - e^+_{-1}) \qquad (4\text{-}8)$$

for each point along the x-axis.

In a practical situation this would be a poor reflector estimator for several reasons. First, the presence of noise in the upcoming wave field makes an estimate based on a single point statistically unreliable. Second, in the case of an incorrect migration velocity the upcoming wave field may not be sharply focused at the reflector. For example, if the migrating velocity were too high

we would naturally expect over-migrated portions of the waves contaminating the region before the first D arrival. Clearly, a practical estimator should accomodate a fuzzy wave front arising from either noise or inaccuracies in the migrating velocity. Thus, we may consider minimizing the weighted sum over M points before the first arrival

$$\min_{C_k} \sum_{i=1}^{M} \omega_i [(1+C_k) e^{+}_{-i} + (1-C_k) e^{-}_{-i}] \qquad (4\text{-}9)$$

A least-squares minimization gives the following estimator of the reflector

$$C_k = \frac{\sum_{i=1}^{M} \omega_i (e^{-}_{-i} + e^{+}_{-i})(e^{-}_{-i} - e^{+}_{-i})}{\sum_{i=1}^{M} \omega_i (e^{-}_{-i} - e^{+}_{-i})^2} \qquad (4\text{-}10)$$

The weights may be chosen depending on the particular problem. The belief that the upcoming waves may be well-focused at $n'=k$ suggests weighting the equations near the reflector more heavily such as with the linear taper $\omega_i = M-i+1$. Thus, from equation (4-7) with $n' < k$ we derive an estimate of the reflection coefficients at depth $k\Delta z$ for all x. Whereas, from the same equations with $n' \geqslant k$ we may compute the upcoming waves U_k using those estimates.

Synthetic Examples

In this section we apply the inverse algorithm developed in the previous section to several synthetic 2-D seismograms. As data we use the results of the forward calculation for the surface boundary conditions. The aim is to numerically verify the theoretical reflector mapping principles and the resulting reflection coefficient estimator.

Figure 4-4 represents the case of two point scatterers imbedded in a constant velocity material. Frame (a) is the original reflector model and frame (b) is the synthetic seismogram taken from Figure 3-5. The inverse source waveform was estimated from the primary and simple multiple of the shallow scatterer by the method of chapter 2. Applying this estimate to the synthetic data yields the surface boundary conditions for D in the downgoing wave equation. The boundary conditions for the upcoming wave U was the unaltered data of frame (b).

Downward continuing both U and D while simultaneously estimating the reflectors we progressively develop the inverse section of frame (c). This may be compared with the original model of frame (a). In both the forward and inverse calculations waves travelling at angles greater than 30° were attenuated in accordance with the narrow beam approximation. Loss of this part of the ω-k spectrum accounts for the inability to completely collapse the primary diffractions. Additionally, the errors in the source waveform estimate contribute to imperfect cancellation of the diffracted multiple reflections. However, even with these numerical inaccuracies the reconstruction is quite acceptable.

A model in which the wave angles are less severe than the previous is illustrated in Figure 4-5. Frame (a) represents an undulating seafloor reflector overlying a faulted monocline. The seismogram as computed with

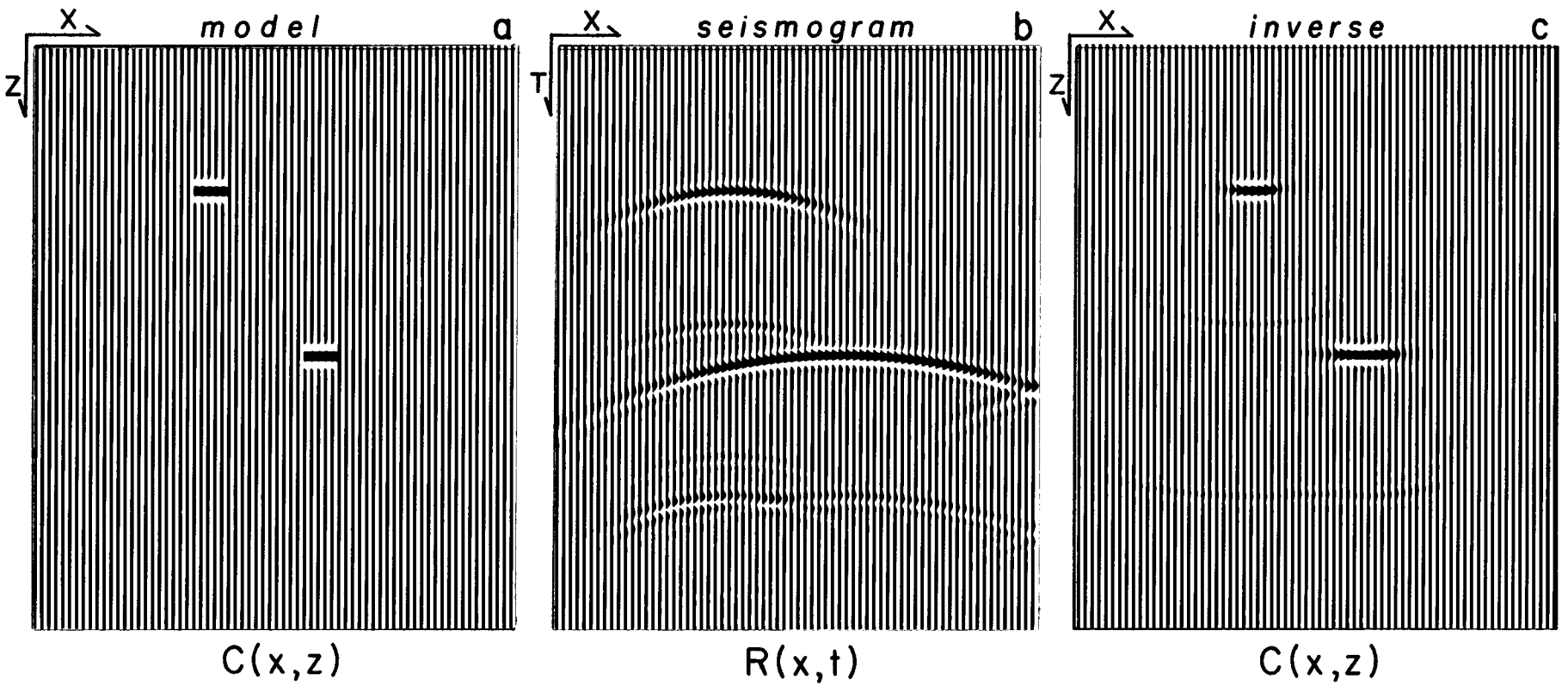

Figure 4-4. Time dependent inversion of two point scatterers in a constant velocity medium. Frame (a) is the original reflector model and frame (b) is the reflection seismogram calculated with the forward 2-D algorithm. This is the same example of Figure 3-5 where recall that the initial disturbance was a plane wave. Using the data of frame (b) as a boundary condition for the differential equations, the waves were projected back down into the earth with the inverse algorithm. Frame (c) is the result of the inversion in attempting to reconstruct the reflectors from the observed diffracted primary and multiple waves. The imperfections in the inversion arise from two sources. First, the difficulty in estimating the inverse source wavelet accounts for the fact that the multiples were not perfectly extinguished. Second, due to attenuation of waves propagating at angles greater than 30° in the calculation some energy is lost. The absence of these angles results in a loss of horizontal resolution as may be noted by the inability to completely collapse the primary diffractions. The vertical exaggeration is 1:1 .

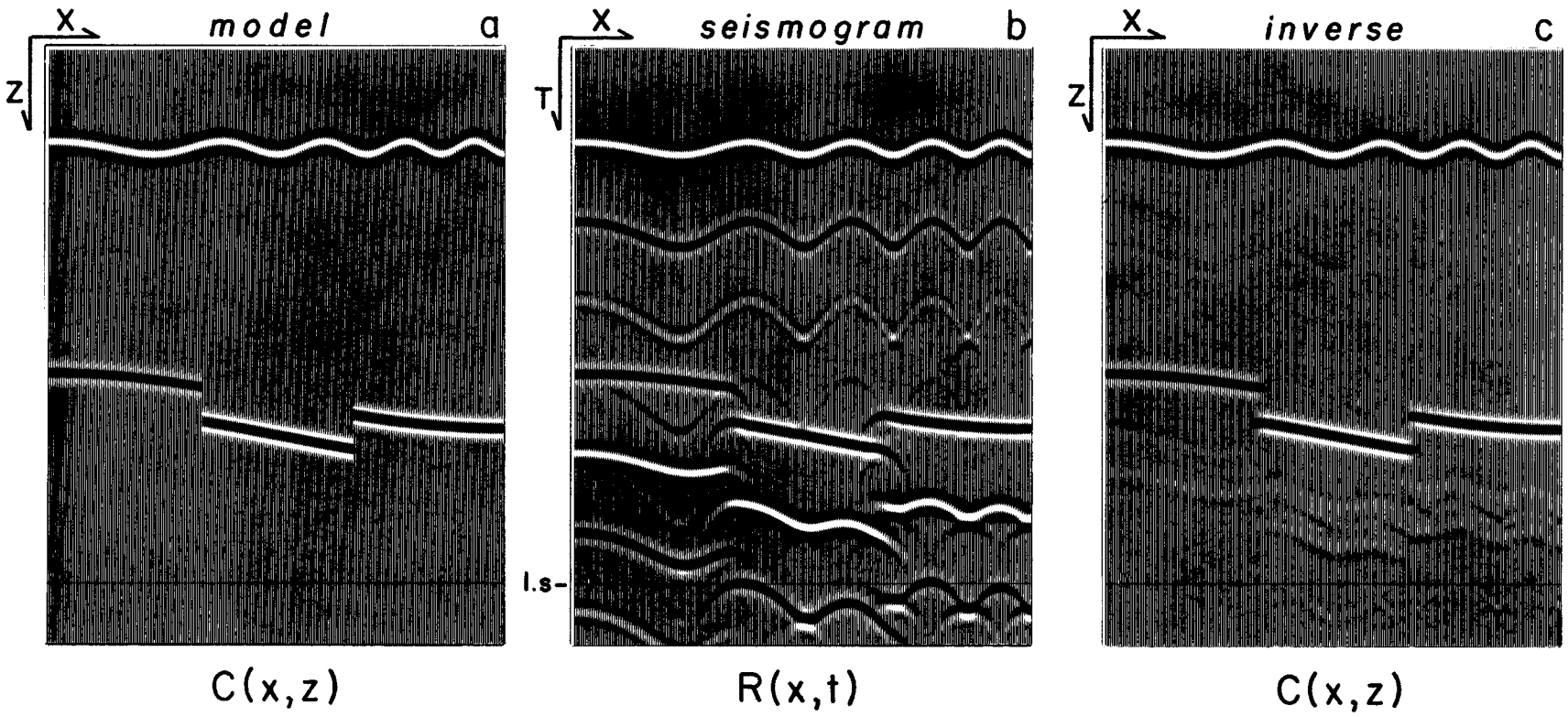

Figure 4-5. Inverse of reflection seismogram due to a rough seafloor and a faulted structure. Frame (a) is the reflector model consisting of a "chirp" seafloor of reflectivity 0.25 overlying a faulted monocline of strength - 0.03 . For the purpose of display, a uniform exponential gain of 36 db/sec. has been applied to all three frames. Frame (b) is the 2-D reflection seismogram computed with the forward algorithm using an initial plane wave source. Note the dramatic difference between the degree of diffraction of the seafloor multiples and the peglegs. Well defined diffractions do not appear until the second seafloor multiple on the right side of the section. However, the first pegleg multiple exhibits considerable focusing and diffraction. Frame (c) is the attempted inversion of the reflection seismogram of frame (b). Note that the diffractions off the fault edges have been properly migrated. The imperfections in the reconstruction are largely due to inaccuracies in estimating the source waveform inverse. The vertical exaggeration is 5:1 .

the forward algorithm is shown in frame (b). Seafloor roughness or curvature increases from left to right, hence the multiple arrivals are more highly diffracted on the right side of the section. This is particularly apparent on the pegleg multiples arriving after the structure primary. It is interesting to compare this calculation to the results of the 1-D synthesis (using the same model) as appeared in Figure 2-5.

With the reflected primary and multiple waves of frame (b) as surface boundary conditions the results of the inverse calculation appear in frame (c). The slight amplitude "halos" in the reconstruction are due to an imperfect source waveform estimate. This does not appear to seriously degrade the ability to invert the diffracted multiples and reconstruct the true reflectors. The important aspect of this example is that the large amount of complex diffracted multiple energy is easily accomodated by the inverse mapping technique. Figure 4-6 illustrates a similar model, however, inaccuracies in this reconstruction are due to a different problem as indicated in the caption.

The final example represents the synthesis and inversion of reflected waves due to a low-velocity ridge structure model. Frame (a) of Figure 4-7 is the reflector time model constructed for a depth model which consists of a low-velocity layer bounded above by a ridge and below by a plane interface (i.e., a planoconvex lens). The surrounding velocity is 1.83 km/sec. and the layer velocity is 1.22 km/sec. The excess low-velocity path beneath the ridge crest is expressed by a 66% velocity pull-down of the lower reflector. Frame (b) is the 2-D reflection seismogram computed with a plane wave source normally incident on the model.

The primary P_a of the top interface scatters waves off the ridge diffusing the recorded wave amplitudes into a wide hyperbola. Waves travelling into the low-velocity layer converge and focus on the lower

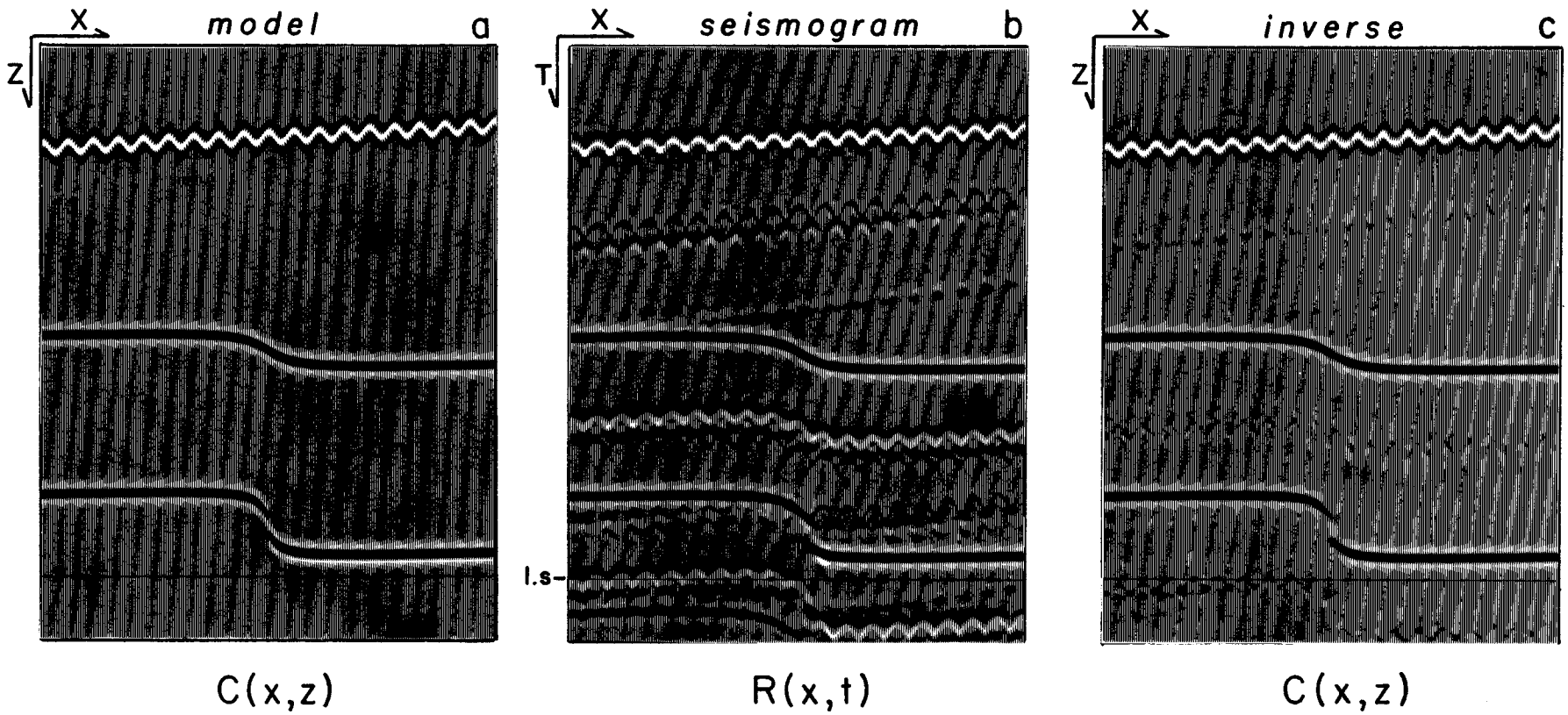

Figure 4-6. Inversion of reflection seismograms resulting from a corrugated seafloor of reflectivity 0.25 overlying a monocline of strength -0.06 and a faulted layer of strength -0.02. For display a uniform exponential gain of 36 db/sec. has been applied. Frame (a) represents the reflector model used in the forward calculation to give the reflection seismogram of frame (b). Note that on the irregular dipping seafloor the amount of diffraction depends on the travel path. Diffraction increases from right to left. Frame (c) is the result of using frame (b) as data for the surface boundary condition in the inverse algorithm. The inability to completely extinguish the diffracted multiples is probably due to not beginning the integration of equations (4-3) far enough after the primaries. Thus, the estimates of the reflection coefficients were based on fuzzy, under-migrated waves. The vertical exaggeration is 5:1 .

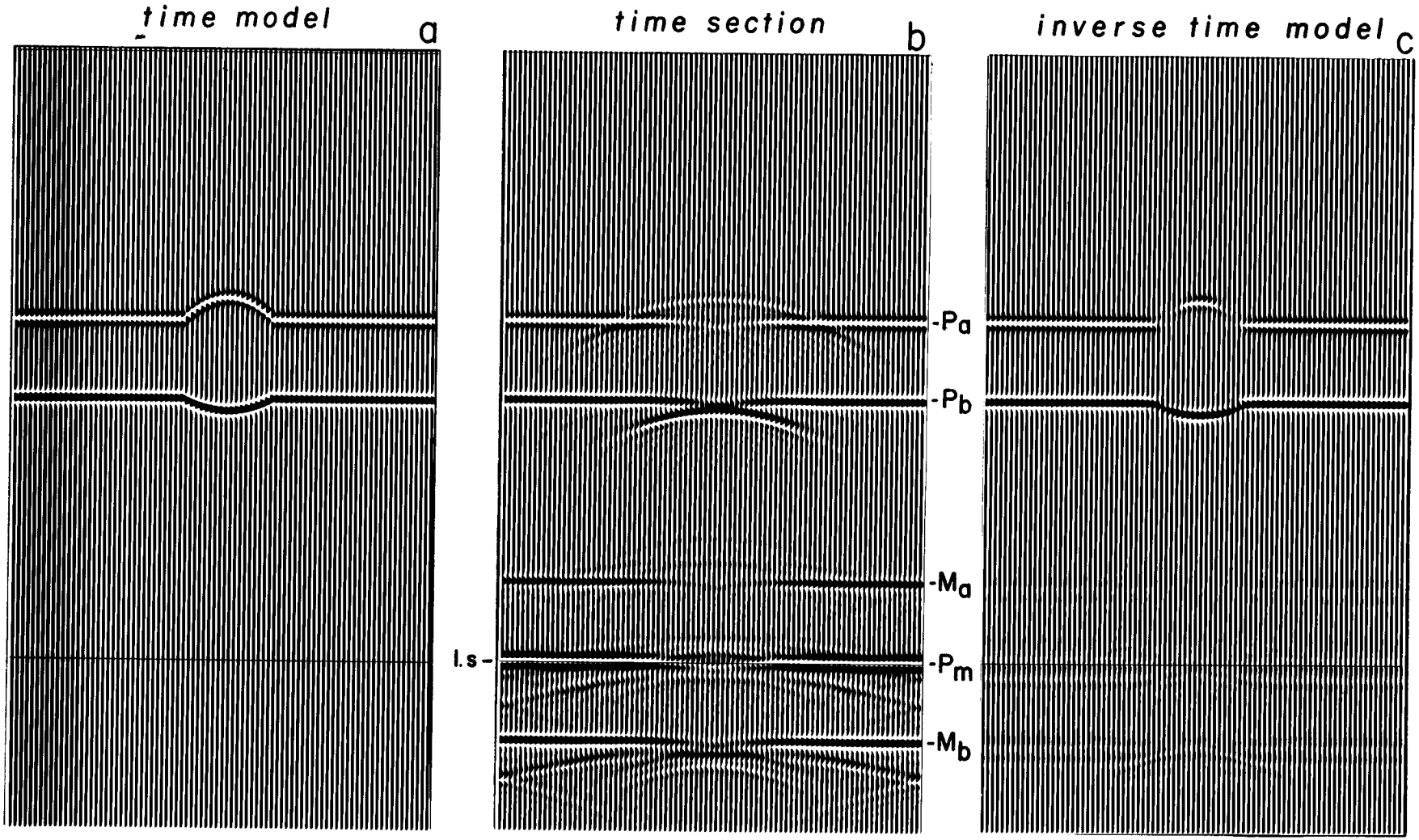

Figure 4-7. Synthesis and inversion of reflected waves due to a low-velocity ridge model. Frame (a): reflection coefficient time section consisting of a ridge overlying a plane reflecting interface. The velocity in the layer is 1.22 km/sec. and the surrounding medium is 1.83 km/sec. The pseudostructure on the lower interface is due to the excess low-velocity path beneath the ridge crest. For a constant density the reflection coefficients are $\pm$ 0.2 . Frame (b): reflection seismogram computed with a normally incident planewave. Frame (c): reconstructed time section as computed with the inverse algorithm using the results of the forward calculation as surface boundary data. Attenuating waves travelling beyond 30° accounts for weak reconstruction of the ridge flanks. Loss of this energy does not seriously degrade inversion of the multiples. The vertical exaggeration is 2.3: 1 .

interface. Reflecting back to the surface, the focused waves then diverge into the travel time hyperbola on P_b .

The multiples for this simple model are strikingly complex. The multiple M_a , having reflected twice off the ridge, diffuses and weakens the reflected amplitudes even further so that the second reflection off the crest is barely visible. The second reflection off the lower interface M_b exhibits refocusing through the lens and further diffraction of the primary P_b wave. The complex pegleg P_m contains several interferring diffracting hyperbolas.

Using frame (b) as the surface data for the inversion, frame (c) is the reconstructed time section as deduced from the waves at depth. Note that the flanks of the ridge are weakened in the migration. This is entirely due to loss of the wide angle waves (ends of hyperbola tails) which have been attenuated by dip filtering in both calculations. However, loss of this energy does not seriously affect inversion of the multiples. The diffracted multiple reflections have been adequately predicted and diminished in the process of downward continuing through the primary structure.

Wave Fields Sampled by Multifold Recording

The forward and inverse problems have been approached assuming that the measurements taken at the surface represent a sufficiently sampled wave field governed by the two-dimensional scalar wave equation. Furthermore, the inverse algorithm was developed assuming an initial plane wave source. The success of this approach to inversion of seismic reflection data depends on the degree to which the data (as surface boundary conditions for the differential equations) fulfill these requirements. This may seem an obvious restatement at this point, however it is of central importance and cannot be overemphasized. Departures of field data from our physical assumptions and numerical approximations are most likely to be associated with 1) preservation of true relative amplitude information, 2) effective source/receiver geometry, and 3) density of sampling in the profiling or x coordinate.

The need for precise amplitude information is not essential for migration of primary reflected waves. However, the inverse techniques (both one and two-dimensional) proposed in this thesis rely upon primary and multiple waves being in accurate and true amplitude balance. AGC type data or poorly recovered binary gain data are insufficient. Further, any correction or stacking operations applied to the data prior to inversion must preserve this relationship.

Marine seismic profiling is normally conducted with a ship towing a repetitive sound source followed by a cable packed with sonic receivers. Typically the cable is 600-2400 m in length with single detectors or sections of summed detectors spaced at 20-50 m intervals. The extent of the cable then represents the aperture within which the reflected wave field is sampled and recorded on separate channels. As the ship

translates along the x-axis , firing the source at regular intervals, the finite cable aperture sweeps out a continuous aperture which may extend for tens or hundreds of kilometers.

Figure 4-8 illustrates the usual multifold recording geometry and resulting aperture coverage due to translating the source and receivers along the x axis . The coordinates of the source and reciever along the x axis are s and g . For a particular s-g pair y represents the midpoint coordinate and f is the separation or offset. By reciprocity y is a plane of symmetry if s and g are interchanged. The coverage of the translating cable aperture is a band of information running parallel and often offset to the midpoint axis. By collecting or gathering the information in this band in various ways we may simulate a variety of synthetic apertures and synthetic source distributions. By summing or stacking the data we may simulate the results of the sources being set off in unison.

A particular gather-and-stack technique in wide use is the common-midpoint stack (common-depth-point stack). This is done by collecting, in the aperture band, data perpendicular to the y axis. These gathers are then moveout corrected, stacked and placed on the y axis. The basic advantage of this stack is the very localized nature of the subsurface coverage. Time stretching of the recordings acts to focus the waves back to a small reflecting region. The fundamental disadvantage, with regards to the inversion procedure of this thesis, is that multiple reflection amplitude information is not preserved.

What we desire is a stacking procedure which faithfully preserves amplitudes and simulates recordings due to a plane wave source. While

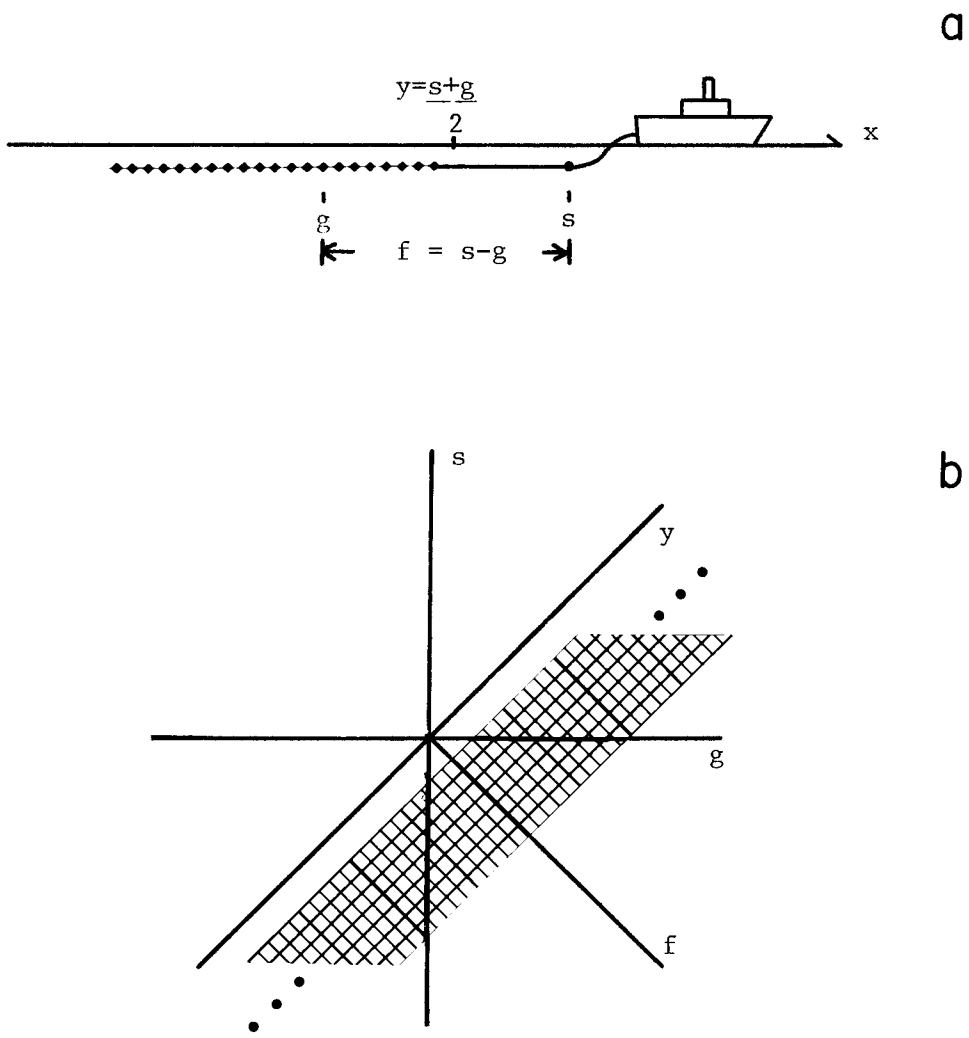

Figure 4-8. Multifold recording geometry and resulting coverage of the cable aperture. a) the ship towing the repetitive source and a cable of receivers sweeps out a continuous region of coverage. The coordinates of the shot and receiver along the x axis are s and g . The midpoint is y and the offset is f . b) As the ship translates along the x axis the data is collected in the hatched region in the s-g plane. Data collected in the aperture band may be used to simulate a variety of other source/ receiver geometries.

we cannot produce a plane source from a linear experiment we may, if the subsurface structure is reasonably 2-D, derive a good approximation from a line source suitably corrected for geometrical spreading into the third dimension. By summing (without normal moveout correction) all possible shots into a common-receiver position we may simulate the results of the shots being fired simultaneously. Repeating this operation for each receiver position yields a representation of the wave field as a function of x due to a linear source. This type of stack, in terms of the available data, is illustrated in Figure 4-9.

Practical problems arise with the common-receiver-point stack when the cable is displaced or offset a large distance from the shot. Under these circumstances the valuable near-vertical incidence waves are lost. Depending on the depth to the reflector and the cable offset this translates into an inability to properly resolve diffractions on the multiples as induced by small lateral variations on the primary waves. That is, small features diffracting the primary wave path may not be encountered on multiple paths. The offset problem may be partially overcome by interpolating traces into zero offset. However, strict application of the inverse technique requires that the wave field be sampled up to vertical incidence.

The final problem which is one not normally considered significant in processing seismic reflection data concerns the sampling of the recorded wave field. The density of sampling determines how well the finite differences of chapter 3 approximate the true derivatives of the waves. Numerical analysts usually state the discretization error in terms of the grid sampling interval. However, a more practical measure is the error associated with a finite grid as expressed in points/wavelength. Fourier transforming the approximations in equations (3-32 a,b,c) we obtain

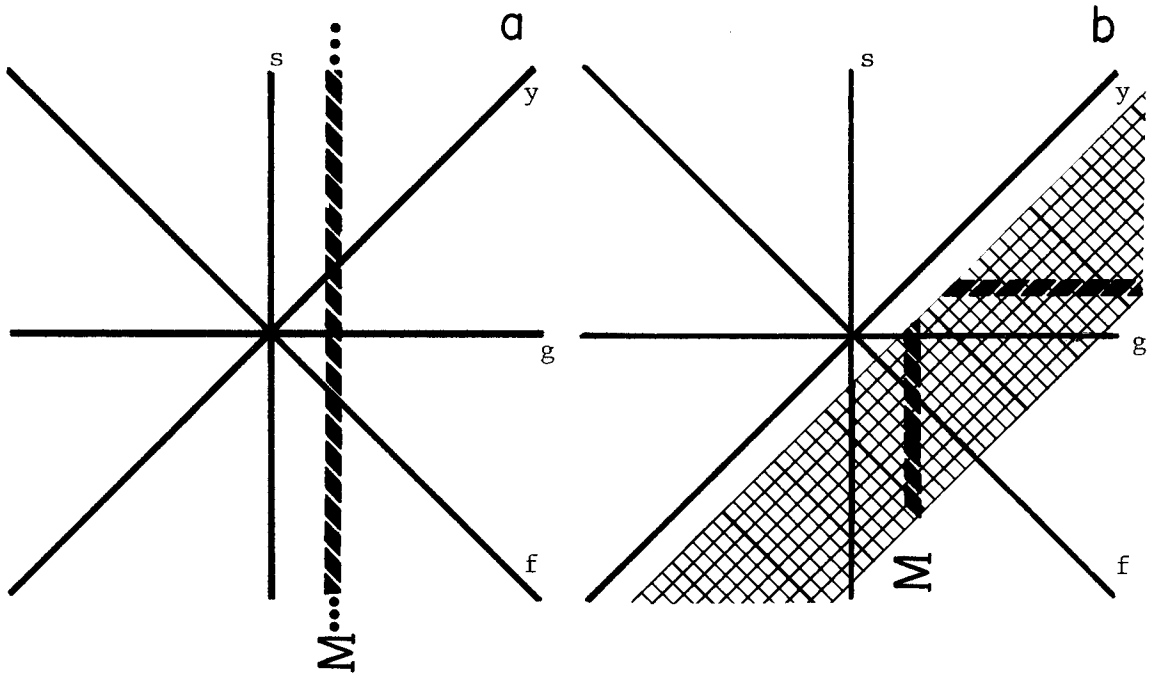

Figure 4-9. Synthesis of a plane wave source. Ideally, if data were collected in all regions of the s-g plane the line source or common-receiver stack would be simulated by summing all recordings (without normal moveout correction) parallel to the s axis along the dashed line of a). Repeating this for each receiver location would simulate the line source (which would then be corrected for geometrical spreading into the third dimension). In terms of the data available in the aperture band of b) this is approximated by summing along the dashed lines. To get the data for negative offset we sum along a line of constant s (by reciprocity interchanging s and g the results are identical, i.e. $U(s,g) = U(g,s)$ implies $U(y,f) = U(y,-f)$).

$$k_z \approx \frac{2}{\Delta z} \tan \frac{k_z \Delta z}{2} \quad , \tag{4-11a}$$

$$\omega \approx \frac{2}{\Delta t} \tan \frac{\omega \Delta t}{2} \quad , \text{ and} \tag{4-11b}$$

$$k_x^2 \approx \frac{4}{(\Delta x)^2} \sin^2 \frac{k_x \Delta x}{2} \quad , \text{ respectively.} \tag{4-11c}$$

Expressing these approximations in terms of η pt/λ in each dimension the discretization errors ε are

$$\varepsilon_{\Delta z}(\eta_z) = (\pi/\eta_z - \tan \pi/\eta_z) \tag{4-12a}$$

$$\varepsilon_{\Delta t}(\eta_t) = (\pi/\eta_t - \tan \pi/\eta_t) \tag{4-12b}$$

$$\varepsilon_{\Delta x}(\eta_x) = (\pi/\eta_x - \sin \pi/\eta_x) \tag{4-12c}$$

If we desire to compute within a 2% error we must have 8 pt/λ in z and t and about 6 pt/λ sampling in x . Usually the waveforms are well sampled in time and the Δz step size may be chosen in the computer to meet this accuracy. Undersampling is most likely to occur along the x axis. For example, at a typical wavelength of 75 m , we would require a Δx no coarser than 35 m to properly model waves up to 20° angles. Clearly the problem may be possibly compounded further for multiple reflected waves. Successive multiple reflections off a dipping interface may rapidly approach steep angles. The correct choice of sampling interval is data dependent, of course, but qualifying the choice must be process dependent. If one expects to apply partial differential equations to field data the sampling must be consistent with the numerical constraints.

Figure 4-10 illustrates a synthetic model computed with the 2-D forward algorithm and two different displays of field data. Frame (a) is the reflector model consisting of a seafloor sloping down into a narrow, flat-bottom depression. For reference, the seismograms computed with the 1-D algorithm are shown in frame (b). The seismograms as computed with the 2-D algorithm and a plane wave source are illustrated in frame (c). Note that with successive reflections off the curved boundary the multiple period shortens. The multiple waves reverberating in the water layer progressively sample higher up the slopes. Thus the multiples migrate upward and inward tending to narrow the width of the depression. By the second multiple M_2 the waves have moved up five wavelengths in the deepest part of the model relative to the 1-D calculation. For a plane wave source there is always a component of the flat bottom in the multiples. This acts to generate a new diffraction hyperbola for each reflection.

Frame (d) is a section of 27-fold common-midpoint stacked field data (CDP) . The model of frame (a) was chosen to closely resemble the migrated seafloor primary of these data. Although the diffractions are partially obscured by other waves the hyperbolic branches may be observed on the first seafloor multiple M_1 . Note also that on the smoothly sloping walls the reverberation period shortens exactly as in the synthetic model. However the discrepancy between the common-midpoint geometry and the plane wave geometry is most apparent in the deep part of the depression. The CDP data do not exhibit rapid narrowing of reflections off the side walls. Although there is some uncertainty as to three dimensional structure, this is probably due to the highly focused nature of the CDP geometry and stack. Due to the differences in wave fields sampled by the two geometries these multiples would not be inverted by the methods in this thesis.

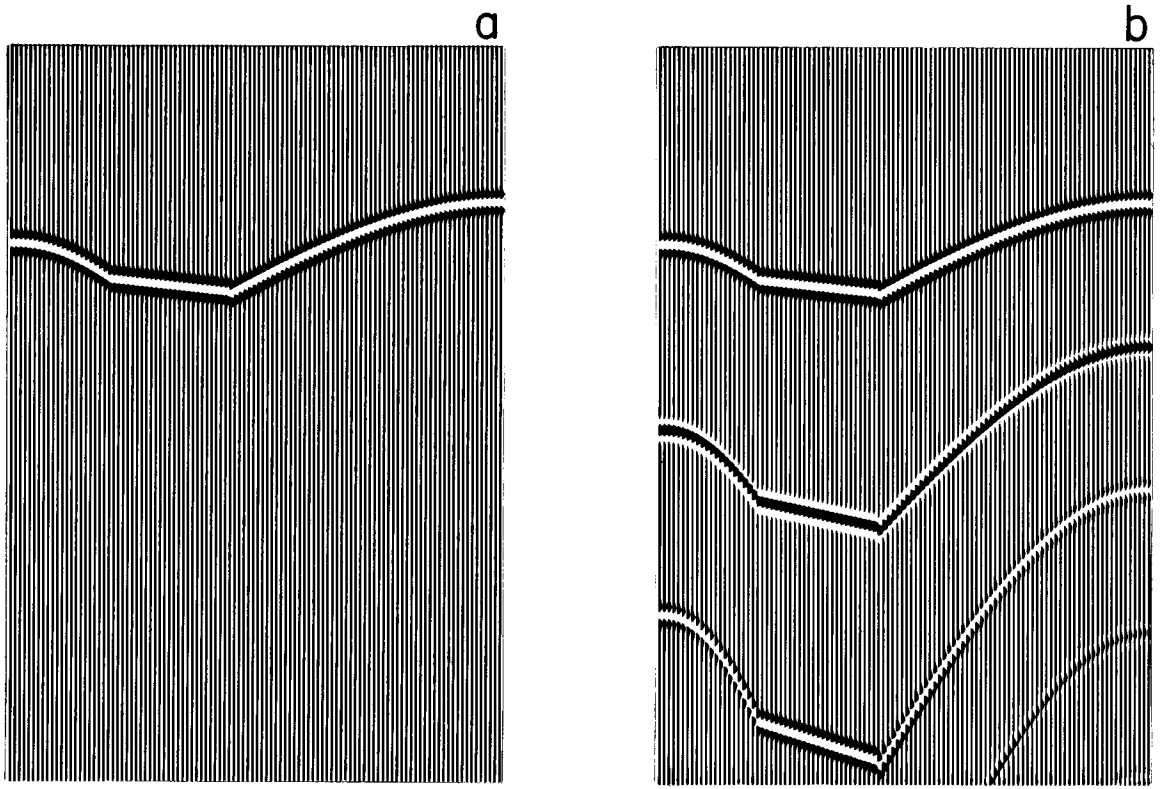

Figure 4-10. Synthetic model and two different displays of field data. Frame (a): reflector model chosen to closely resemble the migrated seafloor of the data in frame (d). Frame (b): 1-D synthetic seismograms. Frame (c): two-dimensional reflection seismogram computed with the forward algorithm and a plane wave source. Frame (d): 27-fold CDP field data. Frame (e): Near-trace section at $f = 170$ m . A comparison of the plane wave and CDP geometry is described in the text.

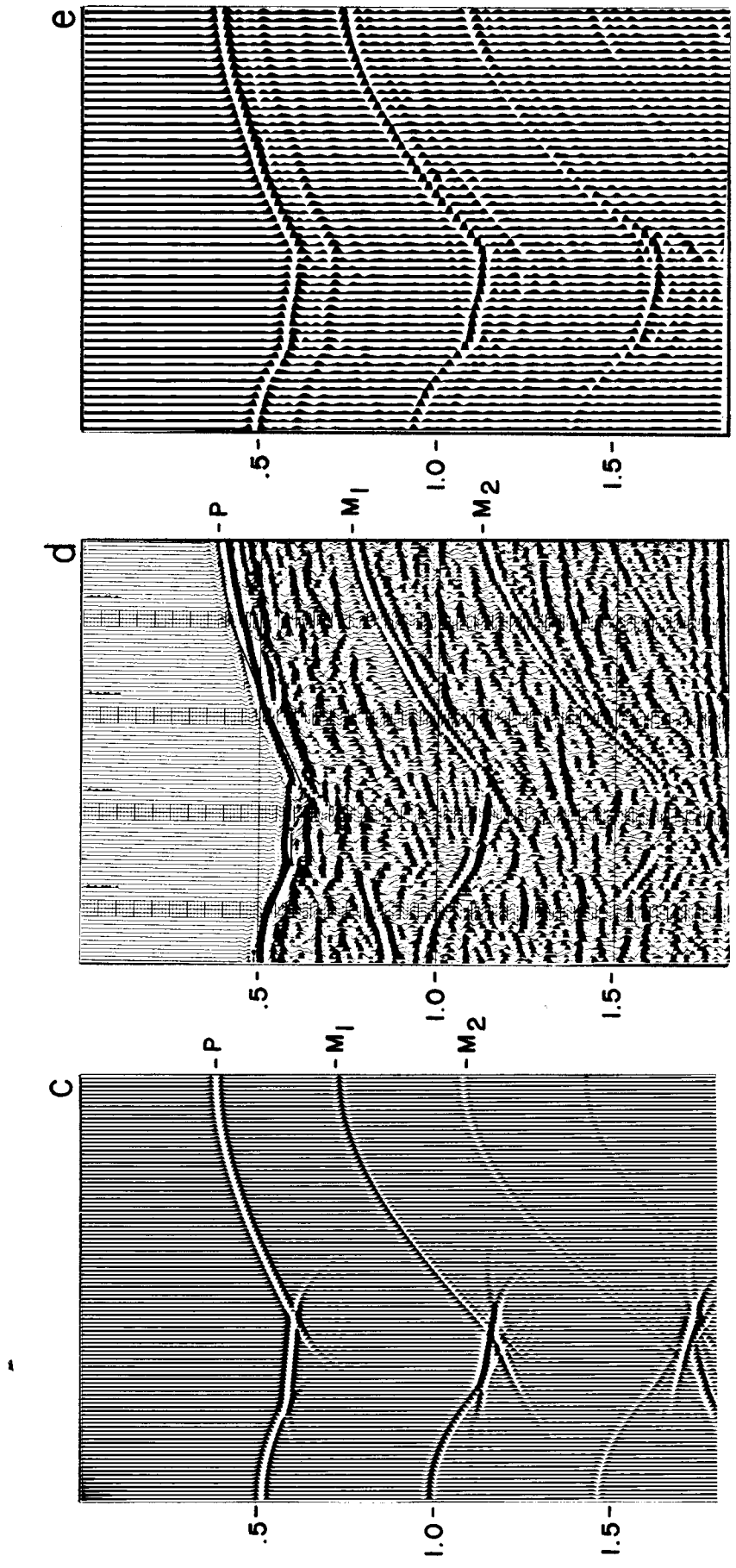

Near Trace Section
same data

27-Fold CDP Section
field data

2-D Synthetic
plane wave source

To illustrate another problem stated above, we note that to properly model waves in this example the spatial sampling interval (Δx) had to be three times as dense as that of the field recordings. For plotting purposes only every third trace computed was displayed in frame (c). That is, to model the waves with about 6 pt/λ in x , Δx was chosen to be 17 m as compared to 50 m spacing of the midpoints in the field recording. Even at this rate some numerical inaccuracies result as may be noted on the steep slope of M_2 . Therefore, even if the physical assumptions were met in this case these data would not be sampled sufficiently for use in the finite difference equations.

These requirements basically relate to possible refinement of field recording procedure or parameters. In particular, the need for true primary and multiple amplitudes and the close offset, small angle waves is essential. Degradation or misrepresentation of amplitudes or the absence of small angles are inconsistent with our underlying assumptions. Experience with data available has consequently proved inconclusive with respect to field application of the inverse theory because of these inconsistencies.